Photometry Technique to Map Elements' Distribution on Comets' Nuclei Surfaces Using a New Method

Ruaa F. Hanash[1a*], Salman Z. Khalaf [1b] and Khaleel I. Abood[2c]

[1]Department of Astronomy and Space, College of Science, University of Baghdad, Baghdad, Iraq
[2]Department of Remote Senescing and GIS, College of Science, University of Baghdad, Baghdad, Iraq
[b]E-mail: salman.zkhalaf@yahoo.com, [c]E -mail: Khaleel.Abod@yahoo.com
[a*]Corresponding author: ruaafarag923@gmail.com

Abstract

This study is unique in this field. It represents a mix of three branches of technology: photometry, spectroscopy, and image processing. The work treats the image by treating each pixel in the image based on its color, where the color means a specific wavelength on the RGB line; therefore, any image will have many wavelengths from all its pixels. The results of the study are specific and identify the elements on the nucleus's surface of a comet, not only the details but also their mapping on the nucleus. The work considered 12 elements in two comets (Temple 1 and 67P/Churyumoy-Gerasimenko). The elements have strong emission lines in the visible range, which were recognized by our MATLAB program in the treatment of the image. The percentage of the elements was determined relative to iron, where in comet Temple 1, the most significant percentage of the element ratio potassium to iron is K / Fe ~ 28.2%, while the lowest value is Ca / Fe ~ 1.3%. For the comet, 67P/Churyumov-Gerasimenko, the most significant percentage of the elements relative to iron is also for potassium, K / Fe ~ 89.5%; while the lowest value is Ni / Fe ~ 0.26. In general, comparing both comets, the greatest percentage of the elements relative to iron is K / F. Iron is the base element in the structure of both comets, followed by potassium.

1. Introduction

The photometric method has many properties to extract more information from any image. This method provides the RGB colors for each pixel in a CCD camera, where each pixel has three colors, and each color has intensity gradients of 0-256. These intensities with the colors give 16,777,215 colors from the number 256 to order 3. From these basics, each color from mixed colors represents one wavelength in the visible range, whereas, in each CCD system, there are three bands in each pixel: red, green, and blue. Each band has an intensity of 0-256, as shown in Fig. 1, the blue color began at 400 nm and peaked at 450nm, and the peak of the green color was at 550 nm, reaching the red color at 700 nm at the end of the visible colors [1-5].

The color in each pixel can be converted to one wavelength in the visible range. Each element has many strong emission lines in the visible range (specific colors in the color line). Any comet or rock that has a mixture of elements can be seen in its nucleus when it is directed at several wavelengths from a target [6-8], where each wavelength represents a different element received from each pixel of the image. This objective then shows the distributions of many elements on its surface.

This work aims to determine the abundance of elements on the surface of the comet nucleus through a picture of this surface and also to determine their mapping on the nucleus.
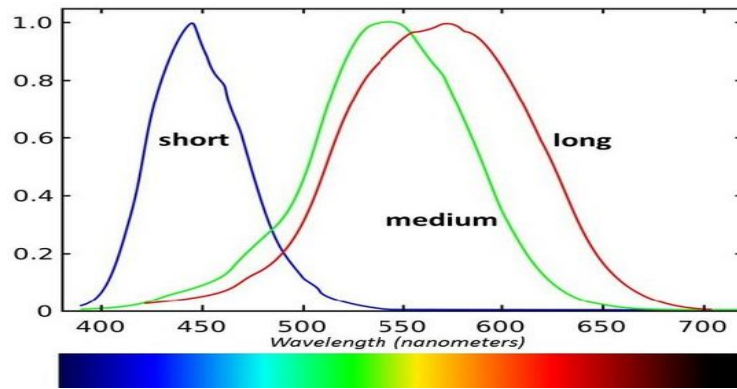
Figure 1: Lines represent the wavelengths of RGB colors [1].

2. Experimental Work
2.1. The Work of Coloration

Almost all comet nuclei have been studied using gray color, and many coloration programs have been used to give the best results for coloring these targets. For example, Fig. 2 shows the comet's nucleus (Temple 1) before and after coloring.
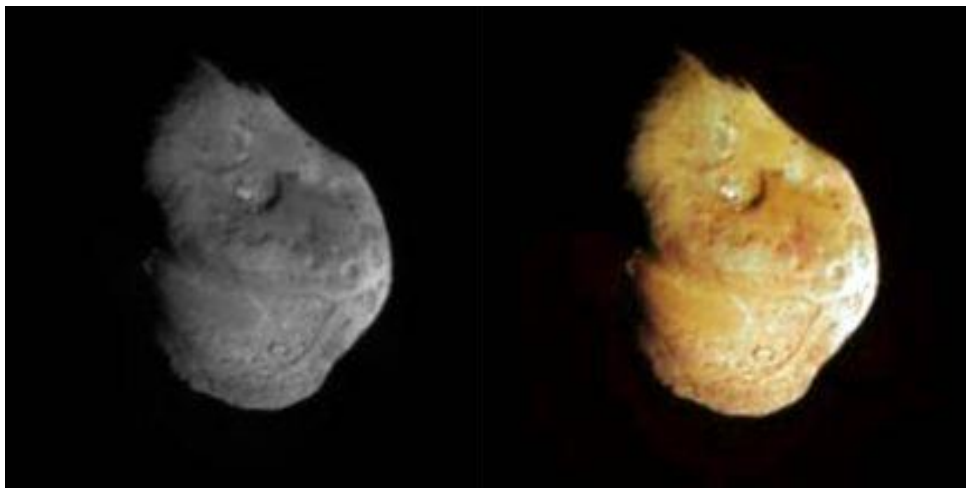
Figure 2: Nucleus of comet Tempel 1 (5 km long) [9, 10].

The colored nucleus gives mixed colors, coming from all elements on its surface. There is a test to acknowledge whether the colors in the new image are false or true. This involves converting the original color image as in Fig. 3(A) [11], to its gray counterpart (no colors), as shown in Fig. 3(B), by using MATLAB and in the order of assistance (gray 2 gray) and then coloring this image with different coloring programs, as shown in Fig. 3(C). The program used for the coloration is Colorize Images, which was downloaded from Google Play.

Some differences in the colors can be noticed between the original image (Fig. 3(A)) and the re-colored image (Fig. 3(C)). The rate of error between the two images was calculated by the role mean square error (MSE) [12-20] using Eq. (1):

$$\text{MSE} = \frac{1}{n}\sum_{i=1}^{n}(P_i - Q_i) \tag{1}$$

where P_i is the original image and Q_i is the image after coloring, where the error was 9%.
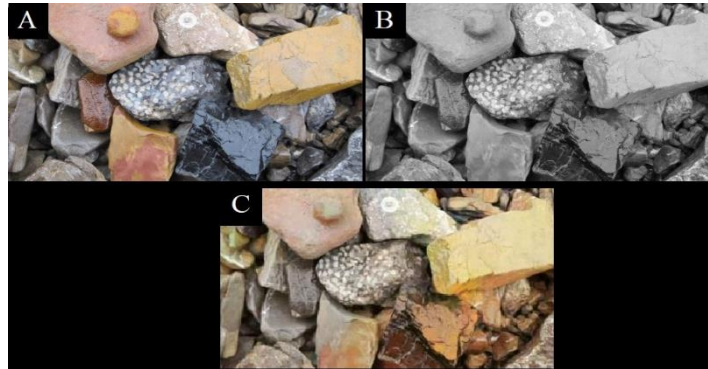
Figure 3: (a) Image of some rocks (original image), (b) gray image by Matlab program, (c) colored image again by a different program.

2.2. Method of Work in MATLAB Program and Some Applications

The early idea of the MATLAB program in its first construction was based on extracting the average wavelength of any laser mono-wave [21-23]. This program was very active in giving the average wavelength of any spot laser. Several applications of this program were demonstrated, where the laser was imaged with a wavelength of 556 nm by the normal camera of our mobile (normal image only), as shown in Fig. 4, and through our analysis program, the spectrum of this image appeared as in Fig. 5.

Figure 4: Spot laser 556 nm.
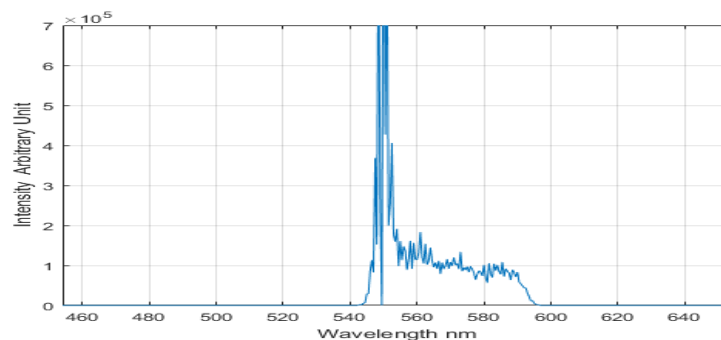
Figure 5: The MATLAB program has experimented with the spectrum of laser 556 nm.

This program gives a rate of error of 1% with this wavelength (556 nm); in addition, it takes the wavelengths of all line bands around this wavelength of the laser. The program was tested for many spots of the wavelengths of many lasers; it was successful in all these tests, as shown in Figs. 6-11 [24, 25].
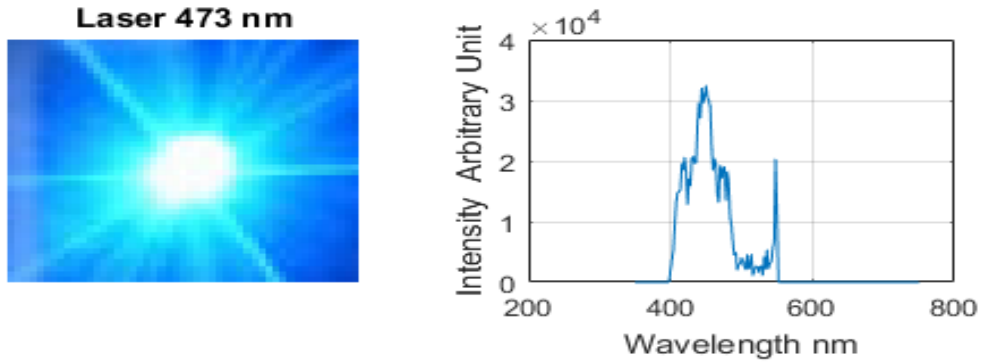
Figure 6: Laser spot 473 nm with error 3.5% by MATLAB program.
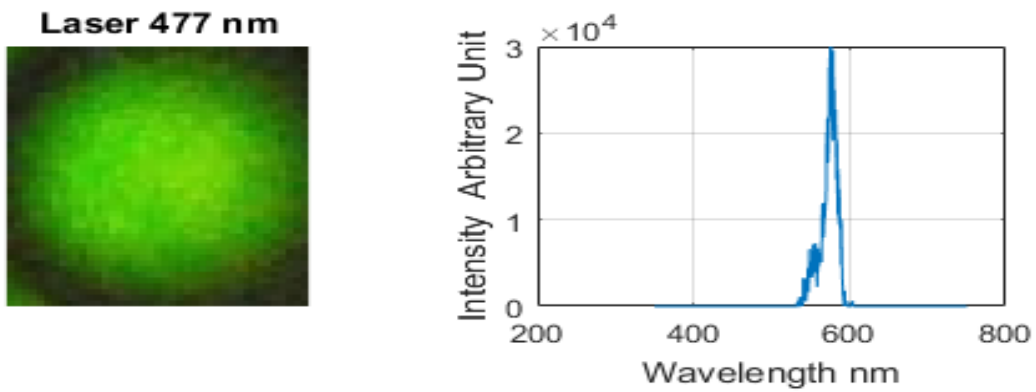
Figure 7: Laser spot 477 nm with error <1%.
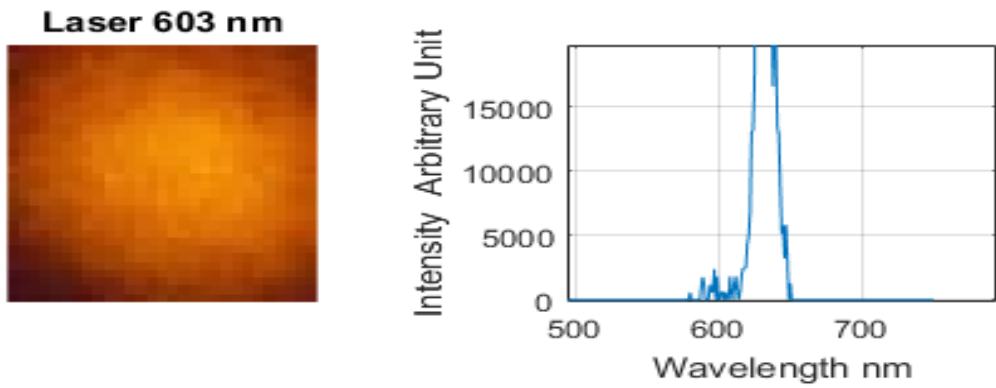
Figure 8: Laser spot 603 nm with error 4%.
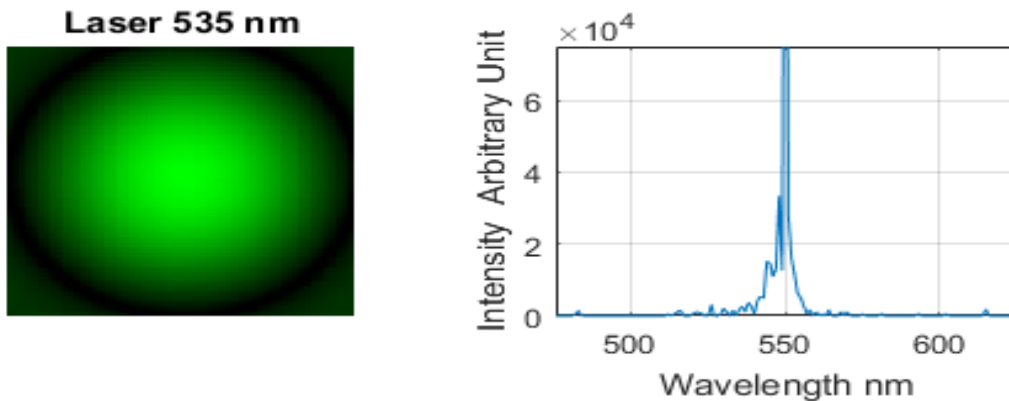
Figure 9: Laser spot 535 nm with error 24 %.
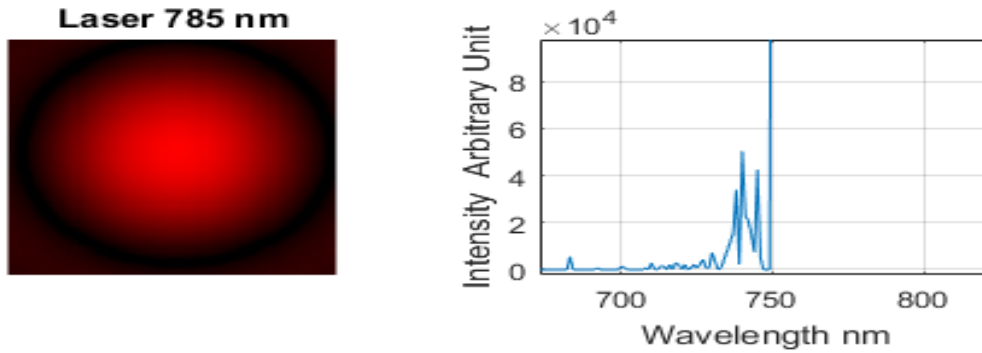
Figure 10: Laser spot 785 nm with error 6 %.
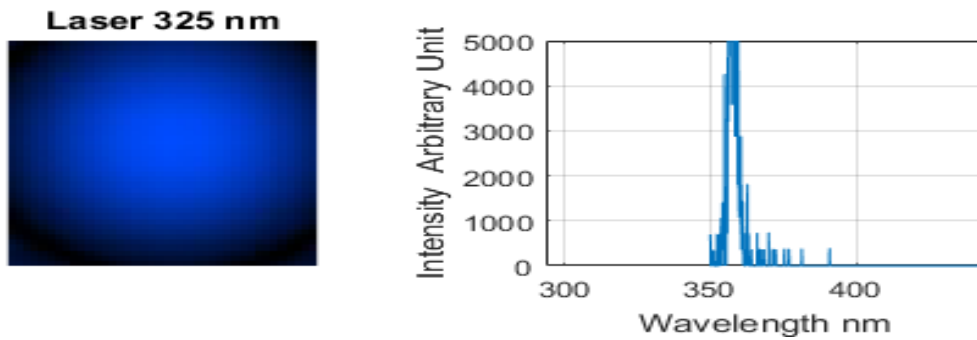
Figure 11: Laser spot 325 nm with error 10 %.

It must be noted that the reference to the above figures is only for the spots of lasers, not for their spectrum. The above examples are some of the experiments of our program with some error in almost all the results; only one has a maximum error of 10%; therefore, the program gives excellent results for the visible range. However, it must be experimented with rocks that contain different elements. The distribution of elements on the surface of any rock can be determined using the program in the visible range.

The reason for choosing rock images was that comet nuclei are rocks and these rocks have elements on their surfaces [26-28]. Rocks that contain gold and silver were chosen because of their distinctive gloss, as shown in Fig. 12. This image was tested in the MATLAB program to determine the reliability of the results in determining the components of this sample, as shown in Fig.13.

Figure 12: shows a rock that contains gold elements in its components [29].
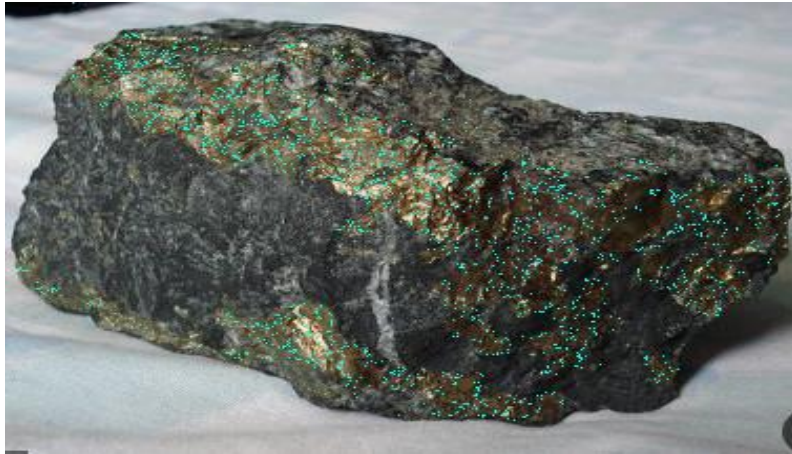
Figure 13: The program accurately determined the gold elments as sit in green spots.

In the figure above, about 1870 pixels out of 102600 pixels appeared (as they appear as green spots in the image), which indicates the existence of a gold element, and the rate of error was 1.8%. The results gave excellent determination of the elements from their wavelengths. Gold has many strong emission lines in the visible range; here, the wavelength of 595.6 nm was used [30, 31].

As shown in Fig. 14, a second rock that contains gold was used to test the program once more.
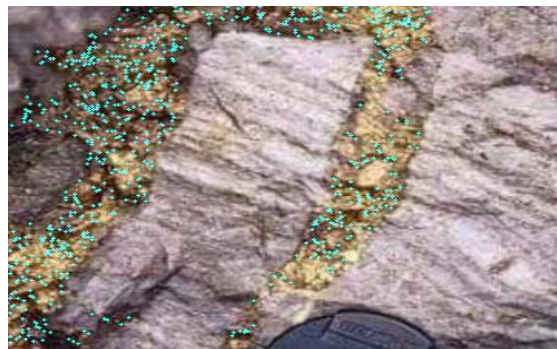
Figure 14: Gold element clear on the surface of the rock [32].

The MATLAB program has determined about 824 pixels from 108000 pixels of the image that have gold at wavelength 595.6 nm with a low error of 0.7%, as shown in Fig. 15. This program was successful in identifying the gold on the rocks.

Figure 15: The green spots indicate to gold element in the rock at wavelength 595.6 nm.

This program was tested for another element (silver). The test was performed on rocks containing silver and gold, as shown in Fig. 16.

Figure 16: Gold and Silver elements under the text by MATLAB program.

Gold and silver have emission lines at wavelengths of 595.6 nm and 547.15 nm, respectively. In the program, the wavelength of an element for the silver element was only 547.15 nm where there are 370 pixels dictated on the silver element and some green spots (around the marker) indicate the area below the element gold, as shown in Fig. 17.
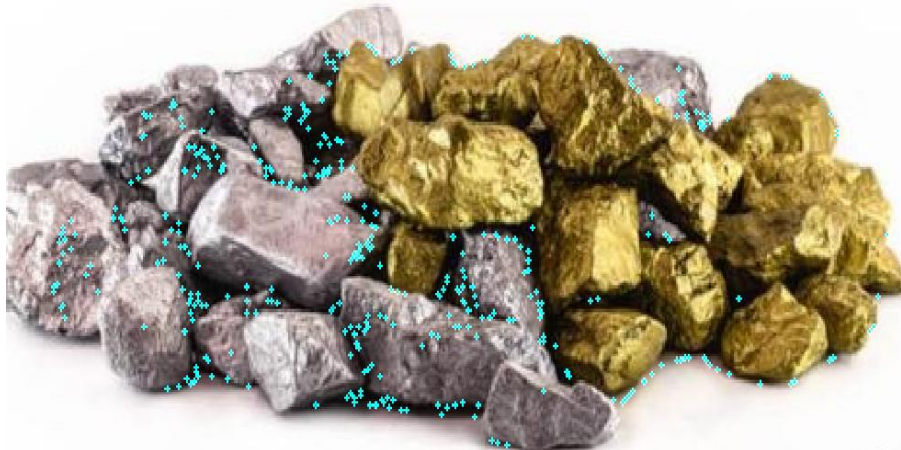
Figure 17: The silver element has λ= 547.15 nm, which has been determined by the MATLAB program with an error of 4%.

3. Determinant of Ion the Elements on the Surface of Nuclei' Comets
3.1. Comet 67P/Churyumov-Gerasimenko

Elements' distributions on the nucleus were determined by developing a new MATLAB program with exceptional mapping on any nucleus' surface face, The nucleus of comet 67P/Churyumoy shown in Fig. 18, was used in this work [33-37].

The image of the 67P/Churyumov-Gerasimeiso comet is gray. This gray image was colored to be analyzed by image processing in the MATLAB program to identify the elements present on its surface, as shown in Fig. 19.
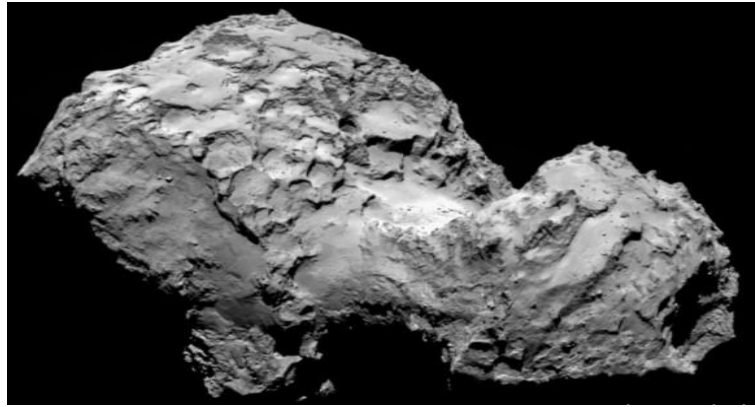
Figure 18: Comet 67P/Churyumov-Gerasimenko on August 3, 2014, as imaged by ESA's Rosetta spacecraft [38].

Figure 19: Nucleus of comet 67P/Churyumov-Gerasimenko after coloraion.

The MATLAB program was designed to read the wavelength of any pixel in the image, or we can calculate an average of all pixels' wavelengths, as shown in Figs. 6-11 of the lasers' spots, where each element has many strong emission lines in the visible range; the program determines the pixels that have these wavelengths in the image. The emission lines for the wavelengths of any element were taken from the NIST site (National Institute of Standards and Technology). Elements' distributions on the comet's nucleus (67P/Churyumov-Gerasimenko) using the MATLAB program are shown in Figs. 20-25. Note: In comet 67P/Churyumov-Gerasimenko, the iron element has 5386 points on the nucleus's surface.
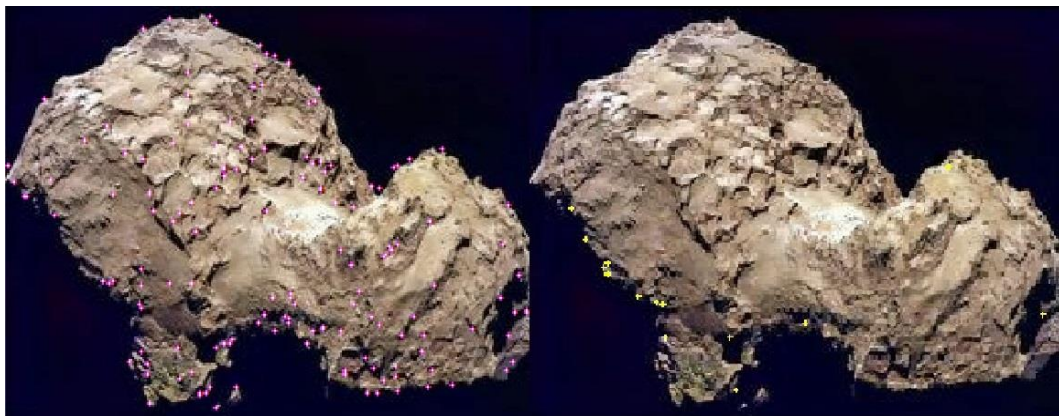
Figure 20: Right image, the distribution of Li/Fe is ~ 2.8%. In the left image, the distribution of Ni/Fe is ~ 0.26.

Figure 21: Right image, the distribution of Ag/Fe of 7.9%. Left image, the distribution of Au/Fe of 8.8%.
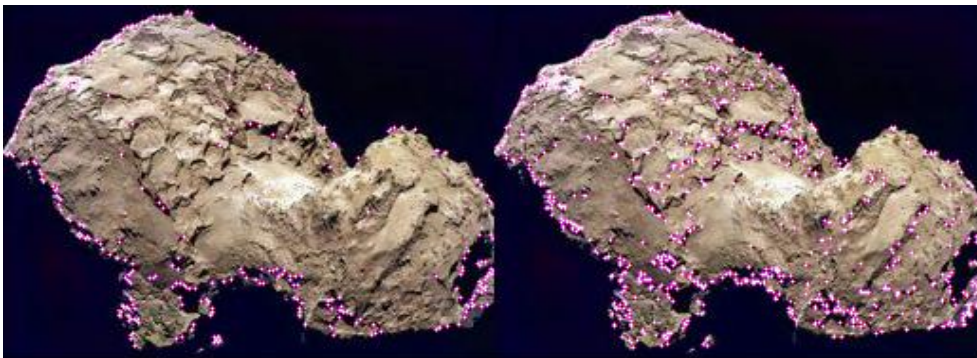
Figure 22: Right image, the distribution of Si/Fe of 15.2%. Left image, Mg/Fe distribution of 5.2%.
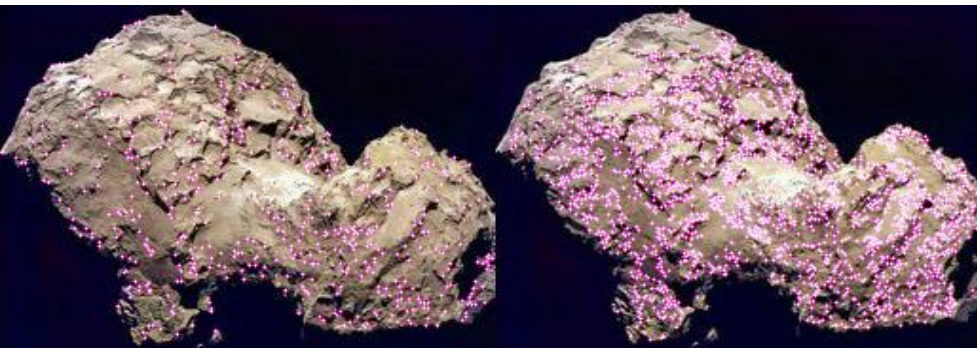
Figure 23: Right image, the distribution of P/Fe of 39.6%. Left image, C/Fe distribution of 8.9%.
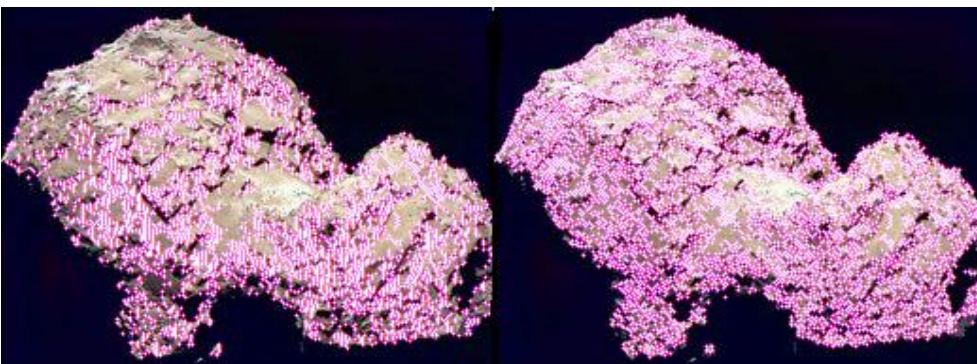
Figure 24: Right image, the distribution of Iron (Fe) in 5 points. Left image, the distribution of K/Fe of 89.5%.
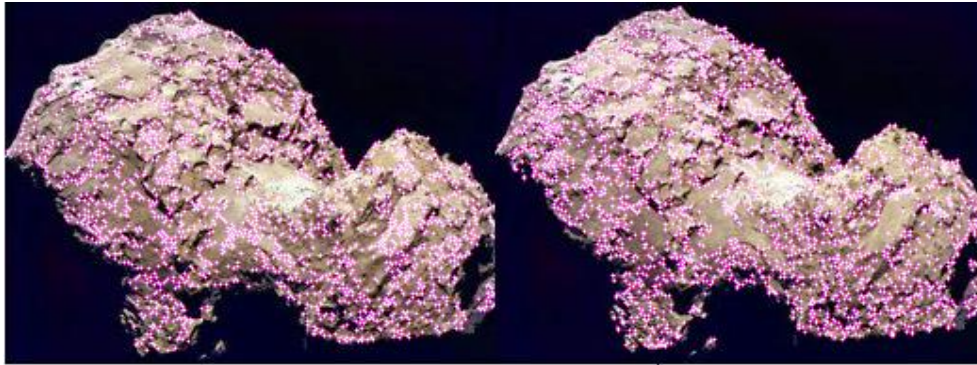
Figure 25: Right image, the distribution of Ca/Fe of 47 %. Left image, Se/Fe distribution of 38%.

3.2 Comet Temple 1

Comet Temple 1 is shown as seen from NASA space on 4 July 2005 [39-45]. The work on this comet was the same as that on comet 76P/ Churyumov-Gerasimenko considering the same elements and comparing both comets. The image of Comet Temple 1 was colored [46-50], as shown in Fig. 26.
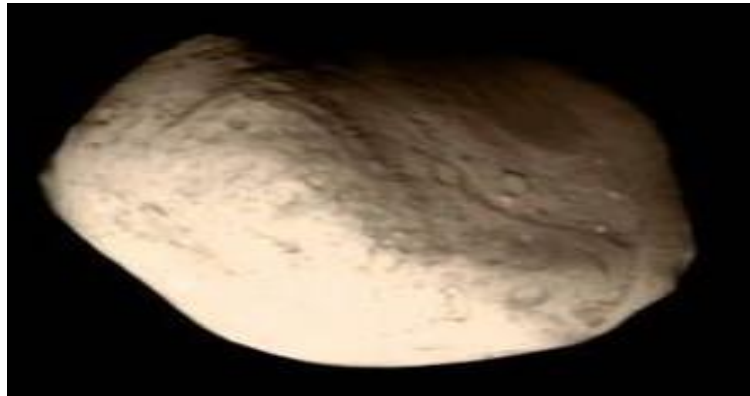
Figure 26: Nucleus of Comet Temple1[39].

The program used the same elements as in comet 67P/Churyumov-Gerasimenko, as shown in Figs. 27-32. In comet Temple 1 the iron element has 7211 points (pixels) on the nucleus's surface from 43758 pixels in the image.
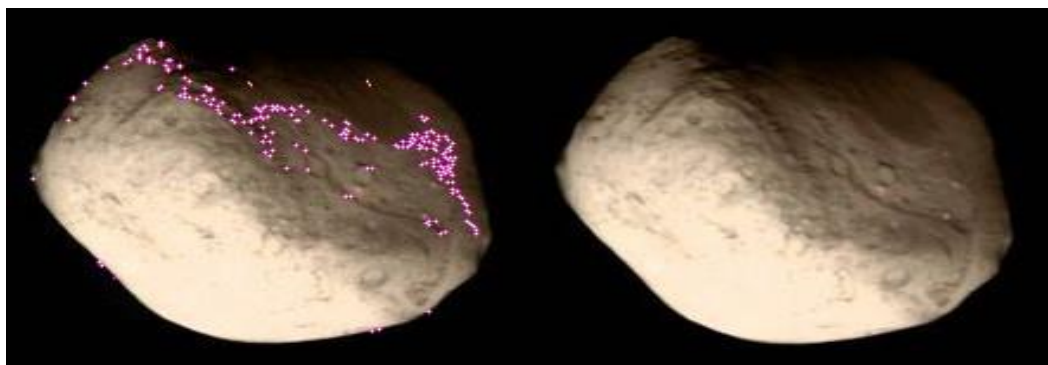
Figure 27: Right image, the distribution of Li/Fe is ~ 3%. Left image, Ni/Redistribution of 0%, this comet has no Nikle element.
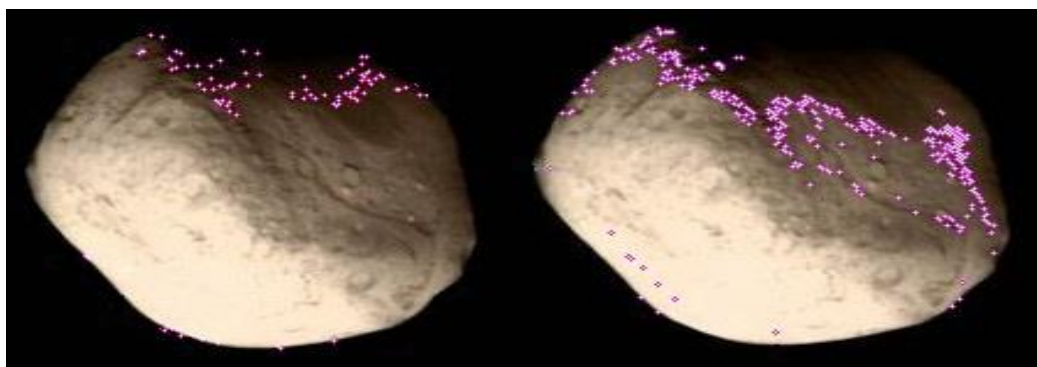
Figure 28: Right image, the distribution of Ag/Fe of 4.8%. Left image, the Au/Fe distribution of 1.8%.

Figure 29: Right image, the distribution of Si/Fe of 25.1%. Left image, the Mg/Fe distribution of 0%, this comet has no Magnesium element.
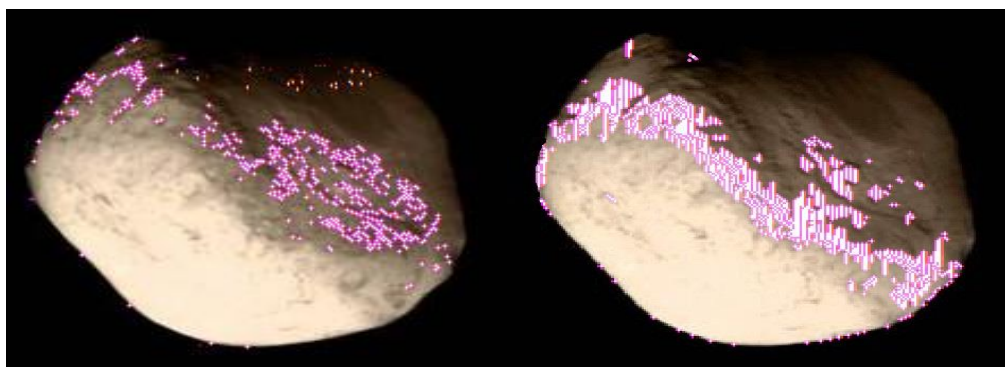
Figure 30: Right image, the distribution of P/Fe of 22.3%. Left image, C/Fe distribution of 7.7%.
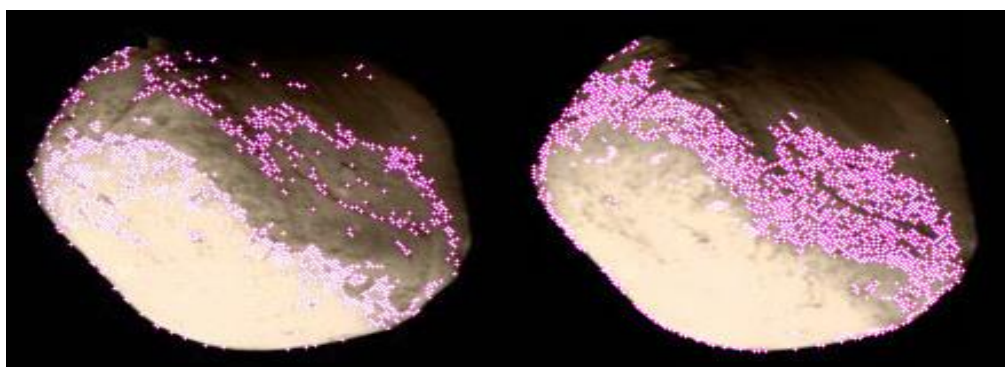
Figure 31: Right image, the distribution of Iron (Fe) in 7211 points. Left image, K/Fedistribution of 28.2%.
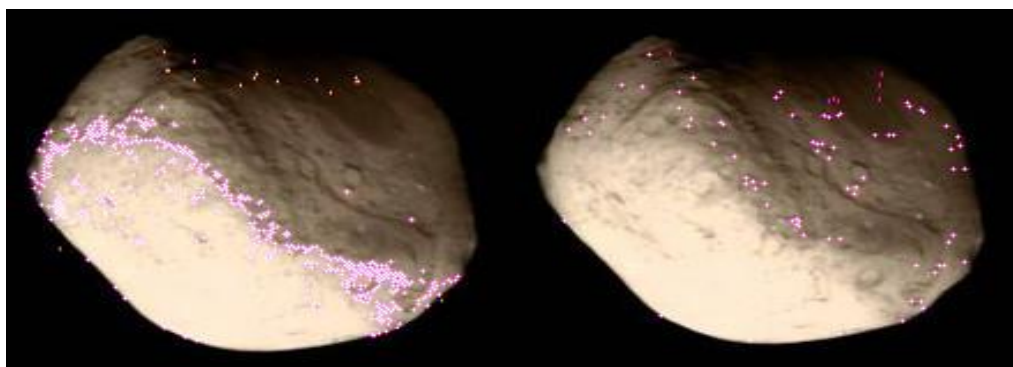
Figure 32: Right image, the distribution of Ca /Fe of 1.3%. Left image, Se /Fe distribution of 8%.

4. Results and Discussion

The reusable lots are represented as a ratio between the elements relative to iron, as shown in Table 1 and Table 2.

Table 1: Ratio of 11 elements relative to iron in Comet 67P/Churyumov-Gerasimenko.

The Element	Li	C	Mg	Si	P	Ca
Element / Fe %	2.80	8.94	5.44	15.20	39.65	47.04
The Element	K	Ni	Se	Ag	Au	
Element / Fe %	89.52	0.26	38.15	7.98	8.83	

Table 2: Ratio of 11 elements relative to iron in Comet Temple1.

The Element	Li	C	Mg	Si	P	Ca
Element / Iron %	3.00	7.70	0.00	25.10	22.30	1.30
The Element	K	Ni	Se	Ag	Au	
Element / Iron %	28.20	0.00	8.82	4.80	1.87	

5. Conclusions

When performing the analysis of comet gases using X-ray sensors in the Chandra satellite, there is a high amount of light elements such as carbon and a few heavy elements because heavy elements (almost metal elements) have strong bonds between their atoms, such as the iron element, where these metal elements have a low volatilization rate, as it occurs with dust coming out of the surface of the nucleus that carries with it small scattered parts of metal elements (heavy elements), so image processing appeared this fact, where light elements such as carbon do not have a high rate among elements, such as gases in a comet coma, where both comets used iron as the largest rating among the elements.

In comet Temple 1 the most significant percentage of the elements' ratio relative to iron was K / Fe ~ 28.2%; while the lowest value was Ca / Fe ~ 1.3%. In comet 67P/Churyumov-Gerasimenko, the most significant percentage of the elements' ratio relative to iron was K / Fe ~ 89.5 %; while the lowest value was Ni / Fe ~ 0.26 %.

In general, when comparing both comets, the greatest percentage of the elements relative to iron was K / Fe. Iron is the base element in the structure of both comets followed by potassium.

Conflict of interest
The authors declare that they have no conflict of interest.

References
1. L. Velho, A. C. Frery, and J. Gomes, *Image Processing for Computer Graphics and Vision*. 2nd Ed. (London, Springer Science and Business Media, 2009).
2. K. H. Abbas, S. Z. Khalaf, and A. A. Selman, Sci. Int. **30**, 729 (2018).
3. S. Khalaf, A. Selman, and E. Al-Lateef, Int. J. Sci. Eng. Res. **4**, 39 (2013).
4. S. Z. Khalaf, Iraqi J. Sci. **48**, 244 (2007).
5. S. Z. Khalaf, A. A. Selman, and H. S. Ali, Al-Nahrain J. Sci. **11**, 80 (2008).
6. A. L. Cochran, H. F. Levison, S. A. Stern, and M. J. Duncan, Astrophys. J. **455**, 342 (1995).
7. J. González, I. Romero, J. Barquinero, and O. García, Mut. Res./Gen. Toxic. Envir. Mutagen. **748**, 60 (2012).
8. A. Springmann, W. M. Harris, E. L. Ryan, C. Lejoly, E. S. Howell, B. E. Mueller, N. H. Samarasinha, L. M. Woodney, and J. K. Steckloff, Planet. Sci. J. **3**, 15 (2022).
9. A. Hanslmeier, *Introduction to Astronomy and Astrophysics*. (Graz, Ausria, Springer Nature, 2023).
10. P. Thomas, M. A'hearn, M. Belton, D. Brownlee, B. Carcich, B. Hermalyn, K. Klaasen, S. Sackett, P. Schultz, and J. Veverka, Icarus **222**, 453 (2013).
11. G. Mavko, T. Mukerji, and J. Dvorkin, *The Rock Physics Handbook*. 3rd Ed. (UK, Cambridge University Press, 2020).
12. D. Salomon, *Coding for Data and Computer Communications*. (Northridge, CA, USA, Springer Science and Business Media, 2006).
13. R. S. Najm, S. Z. Khalaf, and K. I. Abood, Iraqi J. Sci. **64**, 469 (2023).
14. Y. Zhang, T. Sun, C. Wang, L. Ji, J. A. Carter, S. Sembay, D. Koutroumpa, Y. D. Liu, G. Liang, and W. Liu, Astrophys. J. Lett. **932**, L1 (2022).
15. M. A. Cordiner, I. Coulson, E. Garcia-Berrios, C. Qi, F. Lique, M. Zołtowski, M. De Val-Borro, Y.-J. Kuan, W.-H. Ip, and S. Mairs, Astrophys. J. **929**, 38 (2022).
16. F. Manzini, V. Oldani, P. Ochner, E. Barbotin, L. Bedin, R. Behrend, and G. Fardelli, Mon. Noti. Roy. Astronomic. Soci. **506**, 6195 (2021).
17. B. Snios, J. Lichtman, and V. Kharchenko, Astrophys. J. **852**, 138 (2018).
18. D. Bodewits, D. J. Christian, M. Torney, M. Dryer, C. Lisse, K. Dennerl, T. Zurbuchen, S. Wolk, A. Tielens, and R. Hoekstra, Astro. Astrophys. **469**, 1183 (2007).
19. B. Snios, V. Kharchenko, C. M. Lisse, S. J. Wolk, K. Dennerl, and M. R. Combi, Astrophys. J. **818**, 199 (2016).
20. G. L. Betancourt-Martinez, R. S. Cumbee, and M. A. Leutenegger, Astronom. News **341**, 197 (2020).
21. S. Khalaf and M. Jaleel, Int. J. Sci. Eng. Res. **5**, 1231 (2014).
22. S. Z. Khalaf and K. Abrahim, Iraqi J. Sci. **61**, 3417 (2020).
23. S. Z. Khalaf, K. Abrahim, and I. K. Akeab, Iraqi J. Phys. **18**, 21 (2020).
24. M. J. Weber, *Handbook of Laser Wavelengths*. (Berkeley, California, CRC press, 2018).
25. T. Cravens, Science **296**, 1042 (2002).
26. R. Bischoff and M. Mugrauer, Astronom. News **342**, 833 (2021).
27. H. Kobayashi, H. Kimura, and S. Yamamoto, Astro. Astrophys. **550**, A72 (2013).
28. J. Greenwood, I. Williams, S. Smith, and A. Chutjian, Astrophys. J. **533**, L175 (2000).
29. I. Pitcairn, Appl. Earth Sci. **120**, 31 (2011).

30. R. Antoine, Nanomaterials **10**, 377 (2020).
31. G. R. Harrison, *Massachusetts Institute of Technology Wavelength Tables: Wavelengths by element*. Vol. 1. (Massachusetts, USA, MIT Press, 1969).
32. B. Ganse, *The Spacefarer's Handbook: Science and Life Beyond Earth*. 1st Ed. (Berlin, Heidelberg, Springer 2020).
33. S. Benseguane, A. Guilbert-Lepoutre, J. Lasue, S. Besse, C. Leyrat, A. Beth, M. C. Sitjà, B. Grieger, and M. T. Capria, Astro. Astrophys. **668**, A132 (2022).
34. S. Fornasier, H. Hoang, M. Fulle, E. Quirico, and M. Ciarniello, Astro. Astrophys. **672**, A136 (2023).
35. B. J. Davidsson, F. P. Schloerb, S. Fornasier, N. Oklay, P. J. Gutiérrez, B. J. Buratti, A. B. Chmielewski, S. Gulkis, M. D. Hofstadter, and H. U. Keller, Mon. Noti. Roy. Astronom. Soci. **516**, 6009 (2022).
36. B. J. Davidsson, N. H. Samarasinha, D. Farnocchia, and P. J. Gutiérrez, Mon. Noti. Roy. Astronom. Soci. **509**, 3065 (2022).
37. M. Pfeifer, J. Agarwal, and M. Schröter, Astro. Astrophys. **659**, A171 (2022).
38. M. Gargaud and R. Amils, *Encyclopedia of Astrobiology*. Vol. 1. (Floirac, France, Springer Science and Business Media, 2011).
39. M. J. Burchell and E. Johnson, Mon. Not. Roy. Astronom. Soci. **360**, 769 (2005).
40. P. D. Feldman, S. R. Mccandliss, M. Route, H. A. Weaver, M. F. A'hearn, M. J. Belton, and K. J. Meech, Icarus **191**, 276 (2007).
41. G. Milani, G. M. Szabó, G. Sostero, R. Trabatti, R. Ligustri, M. Nicolini, M. Facchini, D. Tirelli, D. Carosati, and C. Vinante, Icarus **191**, 517 (2007).
42. E. Drobyshevski, E. Kumzerova, and A. Schmidt, Astronom. Astrophys. Transac. **26**, 251 (2007).
43. S. I. Ipatov and M. F. A'hearn, Mon. Noti. Roy. Astronom. Soci. **414**, 76 (2011).
44. S. Yamamoto, H. Kimura, E. Zubko, H. Kobayashi, K. Wada, M. Ishiguro, and T. Matsui, Astrophys. J. **673**, L199 (2008).
45. A. L. Cochran, E. S. Barker, M. D. Caballero, and J. Györgey-Ries, Icarus **199**, 119 (2009).
46. L. Kolokolova, L. Nagdimunov, M. A'hearn, A. King, and M. Wolff, Planet. Sp. Sci. **133**, 76 (2016).
47. L. Nagdimunov, L. Kolokolova, M. Wolff, M. F. A'hearn, and T. L. Farnham, Planet. Sp. Sci. **100**, 73 (2014).
48. W. M. Jackson, X. Yang, X. Shi, and A. L. Cochran, Astrophys. J. **698**, 1609 (2009).
49. S. I. Ipatov and M. F. A'hearn, Proce. Int. Astronom. Un. **5**, 317 (2009).
50. M. Ádámkovics, I. De Pater, and H. Spinrad, Astrophys. Sp. Sci. **342**, 309 (2012).

تقنية القياس الضوئي لرسم خريطة توزيع العناصر على أسطح نوى المذنبات باستخدام الطريقة الجديدة

رؤى فرج حنش[1]، سلمان زيدان خلف[1] و خليل أبراهيم عبود[2]

[1] قسم الفلك والفضاء، كلية العلوم، جامعة بغداد، بغداد، العراق

[2] قسم التحسس النائي والمعلومات الجغرافية، كلية العلوم، جامعة بغداد، بغداد، العراق

الخلاصة

هذه الدراسة هي دراسة منفردة في هذا المجال والتي تمثل مزيجا بين ثلاثة فروع للتكنولوجيا، القياس الضوئي، والتحليل الطيفي، ومعالجة الصور لأن هذا العمل يعالج الصورة من خلال معالجة كل بكسل في الصورة بناء على لونها، حيث يمثل اللون طولا موجيا محددا على خط RGB، وبالتالي فإن أي صورة سيكون لها الكثير من الأطوال الموجية من جميع وحدات البكسل الخاصة بها. نتائج الدراسة محددة وتبحث عن العناصر الموجودة على سطح النواة للمذنب، ليس فقط التفاصيل على وجه التحديد ولكن أيضا خرائطها على النواة. أخذ العمل 12 عنصرا في كلا المذنبين (Temple1 و 76P/Churyumoy-Gerasimenko). حيث تحتوي العناصر على

خطوط انبعاث قوية في النطاق المرئي والتي تم التعرف عليها من خلال برنامج MATLAB الخاص بنا عن طريق معالجة الصورة، وبالتالي تم تحديد جميع العناصر للمقارنة فيما يتعلق بعنصر الحديد، حيث في المذنب Temple1، النسبة المئوية الأكثر أهمية لنسبة العنصر بين البوتاسيوم إلى الحديد هي K / Fe ~ 28.2% بينما أدنى قيمة هي Ca / Fe ~ 1.3% ، ولكن في المذنب، P / 67 Churyumov-Gerasimenko، فإن أهم نسبة من العناصر إلى الحديد هي أيضاً عنصر البوتاسيوم، K / Fe ~ 89.5% بينما أدنى قيمة هي Ni / Fe ~ 0.26. بشكل عام مع مقارنة كلا المذنبين فإن أكبر نسبة من العناصر إلى الحديد هي K / F، والحديد هو العنصر الأساسي في بنية كلا المذنبين ثم يأتي عنصر البوتاسيوم.

الكلمات المفتاحية: القياس الضوئي، التحليل الطيفي، المذنبات، معالجة الصور ، نواة المذنب.